Published in final edited form as:
*Cardiovasc Eng Technol*. 2012 March 1; 3(1): . doi:10.1007/s13239-011-0081-3.

# Elevated Strain and Structural Disarray Occur at the Right Ventricular Apex

**V. Hariharan**, **J. Provost**, **S. Shah**, **E. Konofagou**, and **H. Huang**
Department of Biomedical Engineering, Columbia University, 351 Engineering Terrace, 500 W 120th Street, MC 8904, New York, NY 10027, USA

## Abstract

The right ventricular apex (RVA) is a potential hot spot for development of cardiac rhythm anomalies. Many conditions, including arrhythmogenic right ventricular cardiomyopathy and Brugada's syndrome affect the RVA, and further, the RVA remains an incompletely characterized pacing region. Whether there are structural reasons underlying these conduction properties remains unsettled. In the current study, we characterize the mechanical strains and structural attributes of the right ventricular wall, and test the hypothesis that the right ventricular apex experiences heterogeneous strain distributions and altered fiber organization, and is thus susceptible to conduction alterations. Electromechanical wave imaging (EWI), or elastography, of hearts was used to quantify mechanical strains occurring through a cardiac cycle. Histological and immunofluorescence imaging techniques were used to examine cardiac wall structure and arrangement of junctional proteins. Right ventricular mechanical strains were elevated and sustained throughout systole, compared to the left ventricle and septum. Heterogeneous strain distributions, myocardial fiber disarray, and altered junctional protein localization occured at the RVA. Disarray and altered strain distributions suggest decreased structural strength at the right ventricular apex in particular and increased mechanical impositions in the right ventricle, respectively. Thus, these data demonstrate why the right ventricular apex may be particularly vulnerable to conduction abnormalities.

### Keywords

Cardiac structure; Cardiomyopathy; Structure/function; Ultrasound; Elastography

## INTRODUCTION

The right ventricle of the heart is a secondary chamber whose structure is morphologically distinct from the left ventricle. In particular, the right ventricle ‘wraps’ around part of the left ventricle, so that the right ventricular chamber is more crescent-shaped than circular. Because the right ventricle is similar to an ‘added’ wall of the heart, cardiac structure can exhibit discontinuities and experience altered mechanical stresses where the right ventricular lateral wall meets the septum, and in particular at the right ventricular apex (RVA), which must merge with the septum in multiple directions. Because the RVA is a key site for development of arrhythmias and a potential pacing target,[2,3,10] a careful characterization of



Address correspondence to H. Huang, Department of Biomedical Engineering, Columbia University, 351 Engineering Terrace, 500 W 120th Street, MC 8904, New York, NY 10027, USA. hayden.huang@columbia.edu.

CONFLICT OF INTEREST
None

its structure is essential for understanding its role in cardiac physiology. Further, the tendency for arrhythmia development may depend in part on the physical forces being experienced by the RVA region. However, a detailed characterization of the mechanical-structural properties of the RVA, expanding on earlier studies that primarily focus on general fiber orientation within the ventricle itself, may yield new information on the influence of RVA anatomy on the progression of some diseases.[5,17]

For example, Arrhythmogenic Right Ventricular Cardiomyopathy (ARVC) preferentially affects the right ventricular epicardium between the conus arteriosus and ventricular apex, referred to as the 'triangle of dysplasia,' yet reasons for this localization remain unknown.[12,13,19] One study notes the triangle of dysplasia likely represents thinner regions of the right ventricle, but without definitive data.[16] Additionally, the RVA plays a role in other pathologies, such as Brugada's Syndrome, where the RVA is considered an important site for the development of ventricular fibrillation,[4] suggesting that it is a potential hot spot for certain cardiac pathologies. While many such conditions have underlying causes (genetic, molecular, *etc*.) exacerbating their symptoms, the hearts are typically structurally normal when the patient is young. Thus, it is worthwhile examining healthy hearts to determine whether there is any reason underlying the RVA's tendency to be involved in pacing and structural alterations.

Because of a potential interplay between structure and mechanical stresses at the RVA, we propose a biomechanical hypothesis: regions of altered (elevated or heterogeneous) mechanical strains, coupled with structural disarray, may contribute to development of arrhythmias and altered tissue responses, and that these effects are exacerbated in certain disease processes. To test this hypothesis in the context of the RVA, we performed a systematic analysis of the mechanical strains and structural features of the heart, focusing on the RVA region. We examined healthy hearts from canines (suitable for elastography measurements and histological analysis) and rats (suitable for large-scale histological and immunofluorescence analysis) and show that the RVA exhibits persistent elevation and significant gradients in mechanical strains, and diminished organization of a key junctional protein. These results support the 'biomechanical' hypothesis, and explain why the RVA may be predis-posed to initiation of pathological tissue development and represents a hot spot for conduction abnormalities, independently of specific disease processes.

## METHODS

### Elastography

Elastography data was acquired following established protocol.[15] Briefly, two mongrel dogs were anesthetized with injection of thiopental and fitted with standard limb leads for electrocardiogram monitoring. Morphine (0.15 mg/kg, epidural) was administered before surgery, and lidocaine (50 $\mu$g/kg/h, intravenous) was used throughout the procedure. A 0.9% saline solution was supplied intravenously (5 mL/kg/h) to maintain blood volume.

Echocardiography was performed using an Ultrasonix RP system with a 3.3 MHz phased array to acquire RF frames between 390 and 480 frames/s via an automated composite technique.[21] Radial incremental (strain in one frame using the previous frame as reference) and cumulative (change in strain relative to end-diastole) strains in the Eulerian description (motion relative to fixed spatial coordinates) were estimated by applying a least-squares estimator[6] on incremental and cumulative displacements, respectively. Incremental and cumulative strains[8,11] were calculated by taking a spatial average of strains throughout each wall at successive time points, using the roipoly function in Matlab (Natick, MA) to specify the polygonal region of interest. Both whole-wall (WALL; Fig. 2a, outlined in black) and smaller mid-wall regions of interest (MID-WALL; Fig. 2b, black squares) were used for

strain quantification in order to provide large-scale data and variance in radial strain within the region of interest (modified from previous work[11]), respectively. Mid-wall incremental strains were determined using an ROI toward the middle of each wall during the ECG when the peak incremental strain occurred (Figs. 3c, 4c). Normality of the strains within the mid-wall region of interest was confirmed using the Kolmogorov–Smirnov test ($p \leq 0.05$). End-systolic mid-wall cumulative strain was also calculated using a region of interest toward the middle of each wall (Figs. 3d, 4d). Standard errors for regional incremental and cumulative strains were calculated using strain values within each region of interest. Statistical significance was determined using analysis of variance (ANOVA) and Tukey's test.

All animal work was approved by the Institutional Animal Care and Use Committee of Columbia University.

## Histology

Whole rat hearts were extracted via cardiectomy from sacrificed (1-day) post partum adult rats and fixed for 24 h in 4% paraformaldehyde. Septal, left and right ventricular (S, LV and RV, respectively) sections were dissected along the long-axis planes of the heart. Right ventricular sections included myocardium inferior to the apex of the right ventricle, but not extending to the apex of the heart, while left ventricular samples consisted of tissue extending to the apex of the left ventricle, and myocardium from the right ventricular uptract. Septal sections did not include epicardial tissue. Samples were dehydrated with ethanol, cleared with xylene, and embedded in paraffin, taking care to preserve orientation and landmarks to ensure the RVA could be located. Epicardial sections were sectioned into 5 $\mu$m thick samples and mounted on glass slides. Left and right ventricular sections were taken along the epicardial wall, while septal sections were taken from myocardium lining the right ventricle. Sections were subsequently stained using the Chromaview Masson Trichrome Kit (Sigma, St. Louis, MO) according to the manufacturer's protocol, and mounted with Permount Mounting Medium (Fisher Scientific, Waltham, MA).

Canine samples were obtained from formalin fixed whole hearts. Epicardial LV and RVA samples were dissected from the LV wall (toward the apex) and where the RV lateral wall meets the septum, respectively. Samples were processed identically to rat heart samples.

All animal work was performed in accordance with the Institute of Comparative Medicine at Columbia University.

## Structural Analysis

Rat and canine heart histological sections were imaged under bright field microscopy using a 4×, NA 0.13 objective on an Olympus IX-81 microscope (Center Valley, PA). Individual images were assembled using the FIJI plug-in for ImageJ to produce a single high-resolution image of the entire ventricular or septal wall, orienting the apex-base axis vertically with the apex toward the bottom. Line plots were hand-drawn by tracing local fiber orientation, as assessed visually. Lines were omitted at fiber bifurcations and regions where fiber orientation was visually ambiguous. Fiber direction was quantified in septal, left and right ventricular samples with color mapping using Matlab (Natick, MA); a 20 × 20 grid was used to discretize each image into cells where the fiber orientation was determined using a line segment parallel to the local fiber direction. The cosine of each angle was determined in the range of 0–18°, and scaled to a gray-scale map, where horizontal and vertical fibers correspond to black and white, respectively. This map provides a visualization of changes in fiber orientation within a single wall; the greater the changes in fiber orientation, the larger the amount of variance in grayscale. Analysis of fiber direction was performed by determining the percentage of cells within each 20 × 20 grid (Rat $n = 4$; Canine $n = 2$ for

each wall) where the cosine of the angle was greater than 0.3, corresponding to cells with vertically oriented fibers. Statistical significance was determined using ANOVA and Tukey's test for the rat heart samples ($n = 4$), and a Student's *t*-test for canine heart samples ($n = 2$).

### Immunofluorescence

Rat myocardial samples were immunostained using established protocol.[9] Briefly, paraffin-embedded samples were re-hydrated and boiled in citrate buffer (pH 6.0) for 11 min. After cooling to room temperature, tissue sections were concurrently blocked and permeabilized for 45 min (3% normal goat serum, 1% w/v BSA, and 0.15% Triton X-100 in PBS). Samples were then incubated with either mouse-monoclonal anti-plakoglobin (Sigma; 1:400 in blocking buffer) or anti-pan cadherin (Sigma; 1:400) antibody overnight at 4 °C, followed by a 2-h incubation with the secondary antibody (diluted 1:1000) on day two at 25 °C. Fluorescently labeled samples were then mounted with Permount Mounting Medium and imaged using an Olympus IX-81 fluorescence microscope and analyzed using Metamorph and ImageJ. Quantitative microscopy was used to determine JUP and PC signal intensity in regions of fiber disarray relative to regions with uniform fiber orientation. ImageJ was used to threshold fluorescence images to isolate junctional JUP or PC signal, and determine the fraction of pixels above threshold over pixels in the image space. Statistical significance was determined using ANOVA and Tukey's test.

## RESULTS

### Elastography Data Reveal Persistent, Elevated Strain in the Right Ventricle

Elastography measurements of incremental (change from frame to frame) and cumulative (change relative to end-diastole) mechanical strains were acquired along the length of the ventricular walls and septum of a canine heart (Figs. 1a, 1b showing incremental and cumulative strain superimposed on the echocardiography data, respectively). Canine hearts were used due to similarity of their physiology to the human heart, thus being well-suited for elastography measurements.

The RVA exhibits strong sharp changes in the distribution of both incremental strain and cumulative strain (Figs. 2a, 2b). In particular, there are sharp transition regions of strain near the RVA, and especially in Heart 1, peak strains occur near the RVA region. These data suggest that the RVA may be prone to unusual mechanical load distributions due to local load heterogeneity, and in some cases, experience elevated loading.

Quantitative analysis of strain data reveals elevated and sustained incremental and cumulative strains within the RV wall, as compared to the LV wall, during systole (Figs. 3a–3b, 4a–4b). Mid-wall incremental systolic strains are $0.0056 \pm 5.5 \times 10^{-4}$ and $0.0045 \pm 2.2 \times 10^{-4}$ in the right ventricle and $0.0024 \pm 5.3 \times 10^{-5}$ and $0.0017 \pm 4.0 \times 10^{-5}$ in the left ventricle, respectively, corresponding to 133 and 165% increases in incremental strain (Figs. 3c, 4c; $p \leq 0.01$). Mid-wall incremental systolic strains are $0.0043 \pm 1.6 \times 10^{-5}$ and $0.0017 \pm 2.5 \times 10^{-4}$ in the RVA. Since incremental strains represent the change over a short time-span, higher incremental strains suggest a more abrupt load on the myocytes.

Whole-wall cumulative strains during systole are persistently elevated for the right ventricle compared to the left ventricle during systole, although not for diastole (Figs. 3b, 4b). Further, data demonstrate that changes in cumulative systolic strains (end systolic strain minus beginning systolic strain) in the RV wall are greater than that of the LV wall. Mid-wall cumulative end-systolic strains are $0.15 \pm 0.026$ and $0.11 \pm 0.013$ in the right ventricle and $0.094 \pm 0.0058$ and $0.077 \pm 0.0014$ in the left ventricle, representing 1.6 and 1.4-fold

increases in cumulative strain (Figs. 3d, 4d; $p \leq 0.01$). Mid-wall cumulative end-systolic strains are $0.061 \pm 0.010$ and $0.059 \pm 0.007$ in the RVA. Similar elevations are found for diastolic strains. The cumulative strain values obtained for the LV are consistent with those found in literature, from both experimental observations and computational studies, indicating a peak strain of approximately 10% near the basal region of the heart from diastole to systole.[18,20]

These data show that the RV wall bears higher strains for longer periods of time, has elevated changes in strain over short times, and near the RVA, experiences heterogeneity in strain distribution in a small volume. Interestingly, both mid-wall and whole-wall septal cumulative strains are comparable to, or greater than, RV cumulative strains. Additionally, the RVA itself does not exhibit particularly elevated strain magnitudes (incremental or cumulative), compared to the rest of the heart. Thus, elevated, persistent and heterogeneous mechanical strains by themselves are likely not sufficient to explain the RVA as a site for conduction abnormalities.

## Cardiac Fibers at the Right-Ventricular Apex Exhibit Disarray

To examine the structure of the ventricular walls and septum, histological techniques were used to enhance visualization of fiber orientation in samples obtained from rats and canines. Rat hearts were used due to their low epicardial fat and to facilitate the analysis of entire ventricular walls. Due to the thinness of rat heart walls, histological specimens are representative of both epicardium and endocardium.

While disarray is used without formal definition in many cardiac structural studies, in this article disarray refers to abrupt changes in myocyte orientation signifying loss of straight end-to-end coupling. In contrast with the LV and septal regions, myocyte disarray in the RV was a notable recurring theme in the samples, with cell–cell apposition typically occurring at or near the RVA region (Figs. 5a–5c and 5e–5f, left column). There is significant variance in the degree and extent of this disarray, as well as its location. This finding is consistent with the highly variable penetrance of ARVC and arrhythmia development in clinical cases.

To quantify this disarray, histological sections were color-mapped with shades of grey corresponding to the local fiber direction. In the RV, cell–cell juxtaposition ranged from 0 to 90°, whereas a more continuous change in fiber orientation was observed in the LV and septal regions as evidenced by the proximal localization of white and black cells in the gray-scale mapped images of the right ventricle (Figs. 5a–5c and 5e–5f, right column). In the rat RV, 5.7% of cells contained vertically oriented fibers, while left ventricles and septums had 1.1 and 0.7%, respectively (Fig. 5d; $p \leq 0.05$ for LV vs. RV, $p \leq 0.01$ for SEP vs. RV). In the canine RV, 37.75% of cells contained vertically oriented fibers, while left ventricles had 0.375%, respectively (Fig. 5g; $p \leq 0.05$ for LV vs. RV).The right ventricular walls exhibit greater black/white distributions that are either focally located or randomly scattered, suggesting a degree of disarray in the right ventricular walls. In contrast, the left ventricular and septal walls exhibit more uniformity in their gray-box distribution.

## Cell–Cell Junctional Protein Localization is Altered Near the Right-Ventricular Apex

In addition to overt structural disarray in the RVA region, immunohistochemical staining was performed in rat heart sections to assess the localization of both cadherin and plakoglobin at cell junctions. Cadherins are adhesion molecules that hold together adjacent myocytes at their intercalated discs. Plakoglobin is a desmosomal protein that helps link desmin across adjacent myocytes. Plakoglobin is additionally implicated in ARVC, and its expression is altered even in cases where the disease-causing mutation is not in plakoglobin

itself.[1] Thus there is reason to believe that plakoglobin may help stabilize conduction and/or mechanical support pathways.

Far from the RVA, cadherin staining was strong and similar in the left ventricular (Fig. 6a), right ventricular (Fig. 6b) and septal (Fig. 6c) walls, mostly localizing at the end-to-end junctions between adjacent cardiomyocytes. Cadherin signals near the RVA exhibited diminished intensity levels, relative to the rest of the wall, with fiber apposition evident in the RVA region (Figs. 6d, 6f; $p = 0.07$). Plakoglobin also exhibits a similar drop-off in intensity near the RVA ($p \leq 0.05$), suggesting diminished desmosomal expression in addition to fiber disarray (Figs. 6e–6f). Inter-calated disk orientation near the RVA exhibits lower degrees of end-to-end localization and regularity. These results are consistent across the hearts examined. Since desmosomes play a supporting role in gapjunctional architecture, altered electromechanical coupling in this region may account for previously observed idiopathic ventricular arrhythmias in addition to their role in pathologies such as ARVC and Brugada's syndrome.[14]

## DISCUSSION

We show, via tissue-level examination of cardiac structure and mechanical strain that (1) there are persistent, elevated strains and changes in strain over short distances in the right ventricle, during systole, (2) the region near the RVA exhibits structural disarray, and (3) the right ventricular apical region exhibits less organized intercalated disk orientation and diminished desmosomal expression. Our results thus support the “biomechanical” hypothesis and provide an explanation for the preferential development of arrhythmias and, for ARVC, fibrofatty tissue, near the RVA. During systole, when the intramuscle strength needs to be high to maintain tissue cohesion, the right ventricle, and sometimes the RVA, experiences elevated strains, compared to the left ventricle. Further, disarray near the RVA region likely contributes to structural weakness since the lateral adhesion strength of the fibers is likely lower than the end-to-end strength. Thus, heterogeneous fiber orientation, coupled with increased incremental strains, effectively create a “weak spot” in the heart. The diminishment and disorganization of plakoglobin near this region may further weaken the heart or lead to conduction alterations.

While our study does not address a specific disease process, some motivation for examination of the RVA region came from ARVC, which is a leading cause of sudden cardiac death. One primary hypothesis for the etiology of ARVC is that defects in cell–cell adhesion lead to destabilization of cell–cell interactions and disruption of junctional associations. Observations that desmosomal mutations causing ARVC do not generally lead to defects in other desmosome-expressing tissues (with skin/hair involvement being a notable exception) support this hypothesis, since the heart tissue is under persistent, cyclic, elevated mechanical stresses. Our study is consistent with this hypothesis and explains further why the RVA is implicated in other conditions such as Brugada's syndrome and has mixed results as a target for cardiac pacing.

To test our biomechanical hypothesis we did not examine disease model hearts, opting instead to examine cardiac strains and structures to determine how they may contribute to disease development. For example, cardiac structure appears unaltered in the early stages of conditions such as ARVC,[7] manifesting primarily after puberty. Thus, ARVC (and other conduction abnormalities) may not necessarily be the result of *a priori* alterations in cardiac tissue; they may simply initially manifest at hot spots such as the RVA. The variability we report may also explain why ARVC does not always manifest primarily at the triangle of dysplasia (or indeed, necessarily the right ventricle).

Examination of intact bovine hearts revealed a significant fatty deposit around the superior circumference of the heart, some mild fatty streaks following the left-anterior descending coronary artery, and notably, the right-ventricular apical region, but not the primary cardiac apex (unpublished observations). Further, superficial examination of the heart structure shows that the bovine heart RVA region exhibits similar fiber disarray observed in rat hearts. Thus, the phenomenon we report is likely broadly applicable across mammalian hearts and may explain the presence of ARVC-like syndromes in cows and dogs, and provide support for use of different mammalian species in our analysis. Further examination, using more sophisticated techniques (such as diffusion-tensor imaging), direct mechanical testing of the RVA tissue and molecular analysis of RVA mechanotransduction, are warranted. Examination of the other locations of the triangle of dysplasia may be insightful, but were not done in this study because of reduced roles in cardiac conduction issues and difficulty of access for quantitative analysis. Heterogeneity in general fiber disarray and mechanical strains in the present study offer a potential explanation for the varying penetrance in ARVC development as well as variabilities in cardiac pacing using the RVA.[3,10]

The use of Eulerian-based incremental strains was necessitated by the elastography acquisition approach. Further work using multiple angles of approach, in addition to a larger sample size and co-analysis of hearts that are both imaged using elastography and processed for staining, will permit the extraction of three-dimensional strain data and allow a more in depth analysis to support these preliminary findings. Additionally, close examination of the three-dimensional strains around the RVA in particular may be helpful in more precisely characterizing the strain magnitudes and spatial distributions of such strains that may provide more insight into the structure–function relationship of this region.

We show that healthy right ventricles experience elevated strains during systole relative to the left ventricle, and the right-ventricular apex exhibits strain heterogeneity, fiber disarray and diminished plakoglobin expression. Together, this evidence supports the RVA as a hot spot for development of arrhythmias and in particular, the “biomechanical” hypothesis that regions exhibiting both weakened structure and elevated strains are likely to be a focal point for cardiac conduction abnormalities, which may be exacerbated by certain disease conditions.

## Acknowledgments

We thank Mahyar Zoghi for his assistance. This work was supported in part by NIH HL102361, and the National Science Foundation Graduate Research Fellowship.

## ABBREVIATIONS

| | |
|---|---|
| **ARVC** | Arrhythmogenic Right Ventricular Cardiomyopathy |
| **RV** | Right ventricle |
| **LV** | Left ventricle |
| **RVA** | Right ventricular apex |

## REFERENCES

1. Asimaki A, Tandri H, Huang HD, et al. A new diagnostic test for arrhythmogenic right ventricular cardiomyopathy. N. Engl. J. Med. 2009; 360(11):1075–1084. [PubMed: 19279339]
2. Furman S, Schwedel JB. An intracardiac pacemaker for Stokes-Adams seizures. N. Engl. J. Med. 1959; 261:943–948. [PubMed: 13825713]

3. Grover M, Glantz SA. Endocardial pacing site affects left ventricular end-diastolic volume and performance in the intact anesthetized dog. Circ. Res. 1983; 53(1):72–85. [PubMed: 6861298]
4. Hayashi M, Takatsuki S, Maison-Blanche P, et al. Ventricular repolarization restitution properties in patients exhibiting type 1 Brugada electrocardiogram with and without inducible ventricular fibrillation. J. Am. Coll. Cardiol. 2008; 51(12):1162–1168. [PubMed: 18355653]
5. Ho SY, Nihoyannopoulos P. Anatomy, echocardiography, and normal right ventricular dimensions. Heart. 2006; 92:I2–I13. [PubMed: 16543598]
6. Kallel F, Ophir J. A least-squares strain estimator for elastography. Ultrason. Imaging. 1997; 19(3): 195–208. [PubMed: 9447668]
7. Kaplan SR, Gard JJ, Protonotarios N, et al. Remodeling of myocyte gap junctions in arrhythmogenic right ventricular cardiomyopathy due to a deletion in plakoglobin (Naxos disease). Heart Rhythm. 2004; 1(1):3–11. [PubMed: 15851108]
8. Konofagou EE, Fung-Kee-Fung S, Luo J, Pernot M. Imaging the mechanics and electromechanics of the heart. Conf. Proc. IEEE Eng. Med. Biol. Soc. 2006; (Suppl):6648–6651. [PubMed: 17959476]
9. Kwong KF, Schuessler RB, Green KG, et al. Differential expression of gap junction proteins in the canine sinus node. Circ. Res. 1998; 82(5):604–612. [PubMed: 9529165]
10. Leclercq C, Gras D, Le Helloco A, Nicol L, Mabo P, Daubert C. Hemodynamic importance of preserving the normal sequence of ventricular activation in permanent cardiac pacing. Am. Heart J. 1995; 129(6):1133–1141. [PubMed: 7754944]
11. Lee WN, Provost J, Fujikura K, Wang J, Konofagou EE. In vivo study of myocardial elastography under graded ischemia conditions. Phys. Med. Biol. 2011; 56(4):1155–1172. [PubMed: 21285479]
12. Lobo FV, Heggtveit HA, Butany J, Silver MD, Edwards JE. Right ventricular dysplasia: morphological findings in 13 cases. Can. J. Cardiol. 1992; 8(3):261–268. [PubMed: 1576560]
13. Marcus FI, Fontaine GH, Guiraudon G, et al. Right ventricular dysplasia—a report of 24 adult cases. Circulation. 1982; 65(2):384–398. [PubMed: 7053899]
14. Navarrete A. Idiopathic ventricular tachycardia arising from the right ventricular apex. Europace. 2008; 10(11):1343–1345. [PubMed: 18755756]
15. Provost J, Lee WN, Fujikura K, Konofagou EE. Electromechanical wave imaging of normal and ischemic hearts in vivo. IEEE Trans. Med. Imaging. 2010; 29(3):625–635. [PubMed: 19709966]
16. Sen-Chowdhry S, Lowe MD, Sporton SC, McKenna WJ. Arrhythmogenic right ventricular cardiomyopathy: clinical presentation, diagnosis, and management. Am. J. Med. 2004; 117(9): 685–695. [PubMed: 15501207]
17. Sheehan F, Redington A. The right ventricle: anatomy, physiology and clinical imaging. Heart. 2008; 94(11):1510–1515. [PubMed: 18931164]
18. Takayama Y, Costa KD, Covell JW. Contribution of laminar myofiber architecture to load-dependent changes in mechanics of LV myocardium. Am. J. Physiol. Heart C. 2002; 282(4):H1510–H1520.
19. Thiene G, Nava A, Corrado D, Rossi L, Pennelli N. Right ventricular cardiomyopathy and sudden death in young people. N. Engl. J. Med. 1988; 318(3):129–133. [PubMed: 3336399]
20. Usyk TP, Mazhari R, McCulloch AD. Effect of laminar orthotropic myofiber architecture on regional stress and strain in the canine left ventricle. J. Elasticity. 2000; 61(1–3):143–164.
21. Wang SG, Lee WN, Provost J, Luo JW, Konofagou EE. A composite high-frame-rate system for clinical cardiovascular imaging. IEEE Trans. Ultrason. Ferroelectr. Freq. Control. 2008; 55(10): 2221–2233. [PubMed: 18986870]

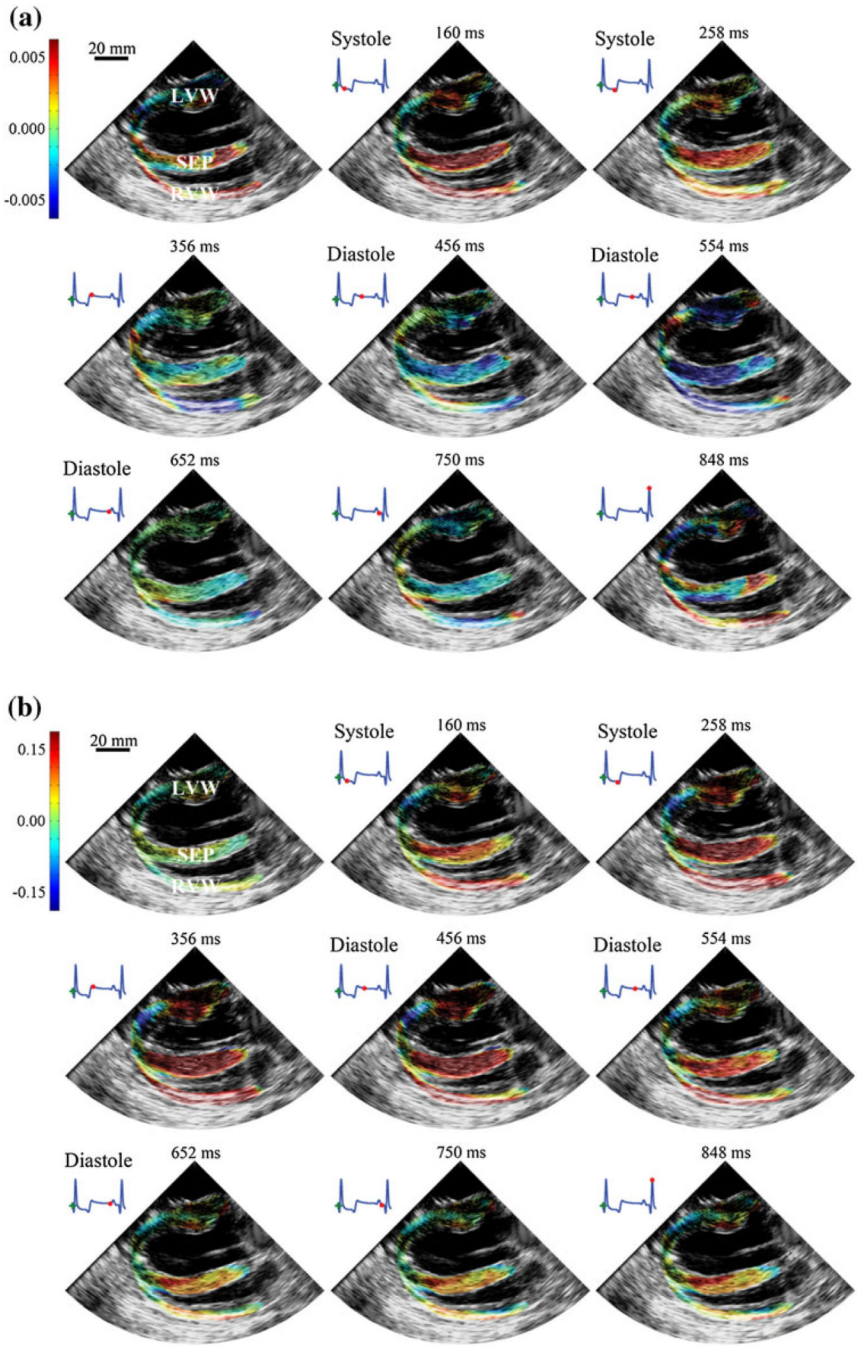


**FIGURE 1.**

Spatial distribution of (a) incremental and (b) cumulative radial strains, superimposed on echocardiogram, across canine ventricular walls at different time points in one complete ECG cycle (denoted by red dots). The left ventricular wall (LVW) is shown at the top of the image, followed by the septum (SEP) in the middle and the right ventricular wall (RVW) at the bottom. Both incremental and cumulative strains are superimposed against the acquired echocardiography data.

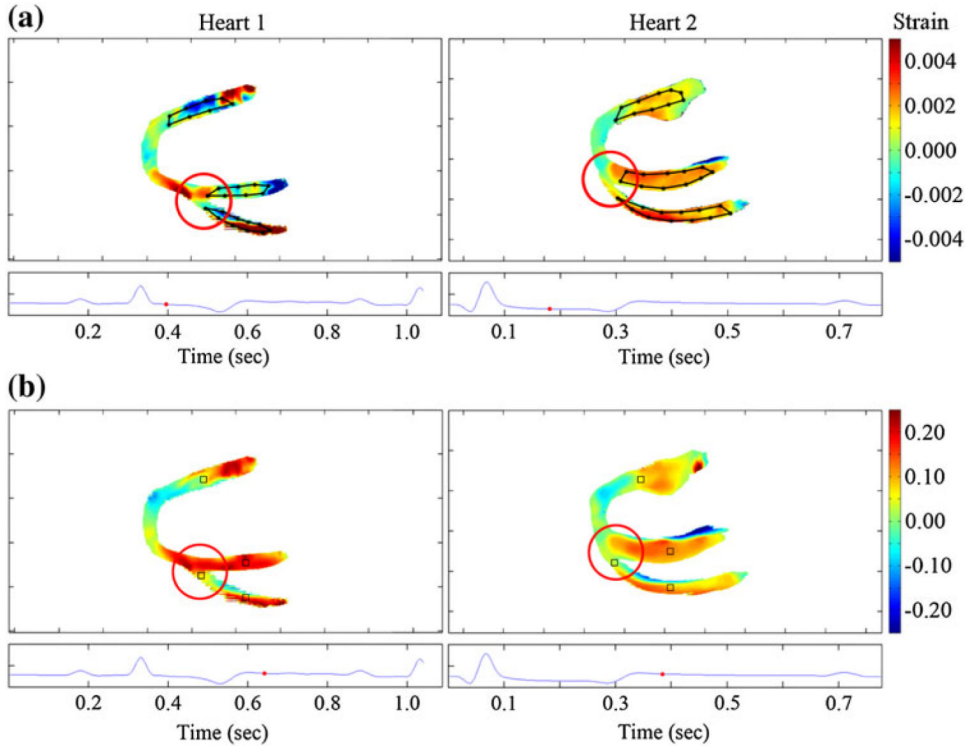


**FIGURE 2.**

Spatial distribution of (a) incremental strains during systole and (b) cumulative radial strains near the beginning of diastole, showing a transition in strain magnitude near the RVA (circled in red), over a short distance compared to a similar transition over the cardiac apex. Black outlines (a) are used to identify regions used for whole-wall strain analysis. Black squares (b) are used to identify regions used for mid-wall strain analysis.

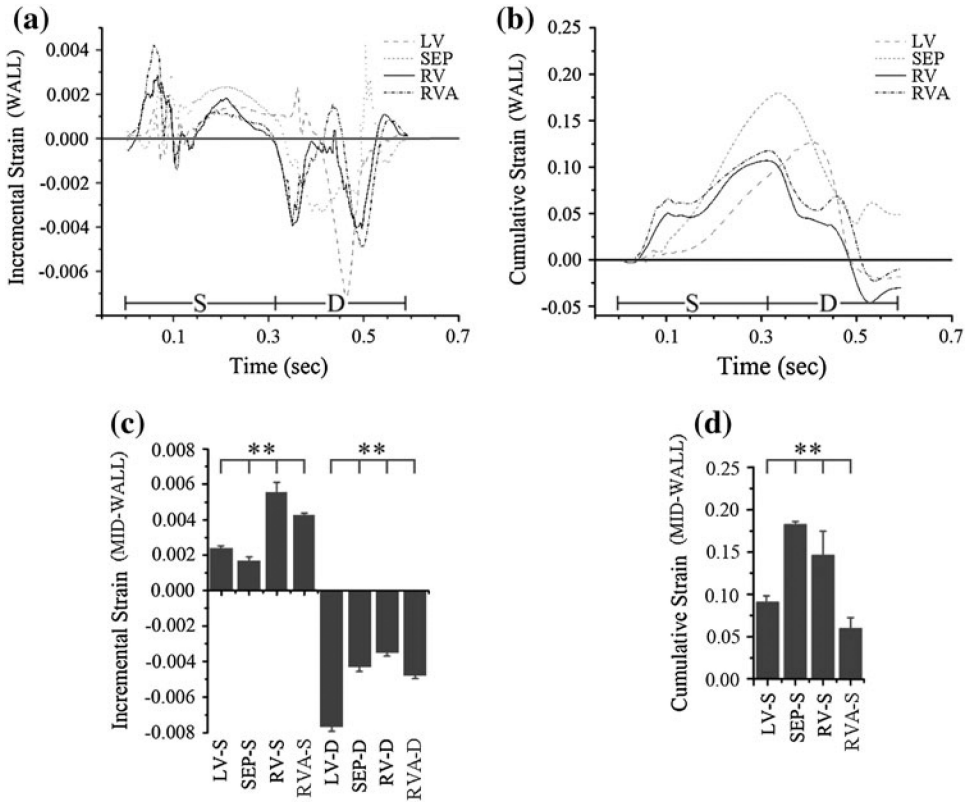


**FIGURE 3.**

Incremental (a) and cumulative (b) strains within canine Heart 1 during systole (S, 0–310 ms) and diastole (d, 310–595 ms). Sustained, elevated strains are observed within the right ventricle (RV) as compared to the left ventricle (LV) during systole. Mid-wall incremental strains (c) and end-systolic mid-wall cumulative strains (d) show elevated RV strains compared to LV strains. $^{**}p \leq 0.01$.

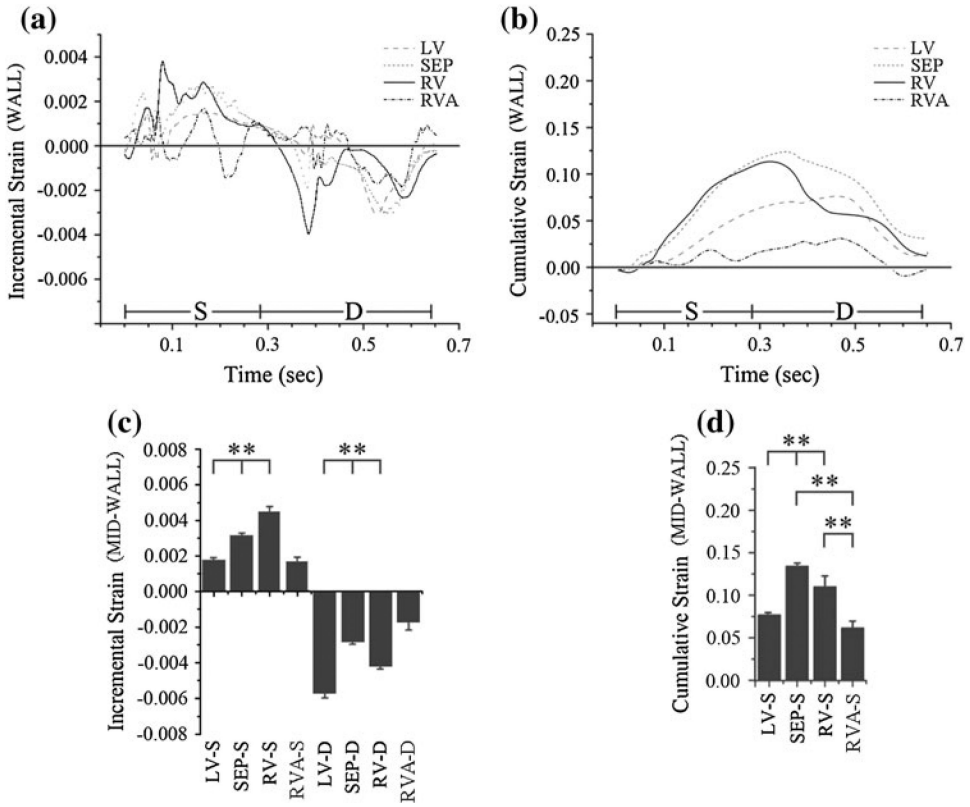


**FIGURE 4.**

Incremental (a) and cumulative (b) strains within canine Heart 2 during systole (S, 0–290 ms) and diastole (D, 290–645 ms). Sustained, elevated strains are observed within the right ventricle (RV) as compared to the left ventricle (LV) during systole. Mid-wall incremental strains (c) and end-systolic mid-wall cumulative strains (d) show elevated RV strains compared to LV strains. $^{**}p \leq 0.01$.

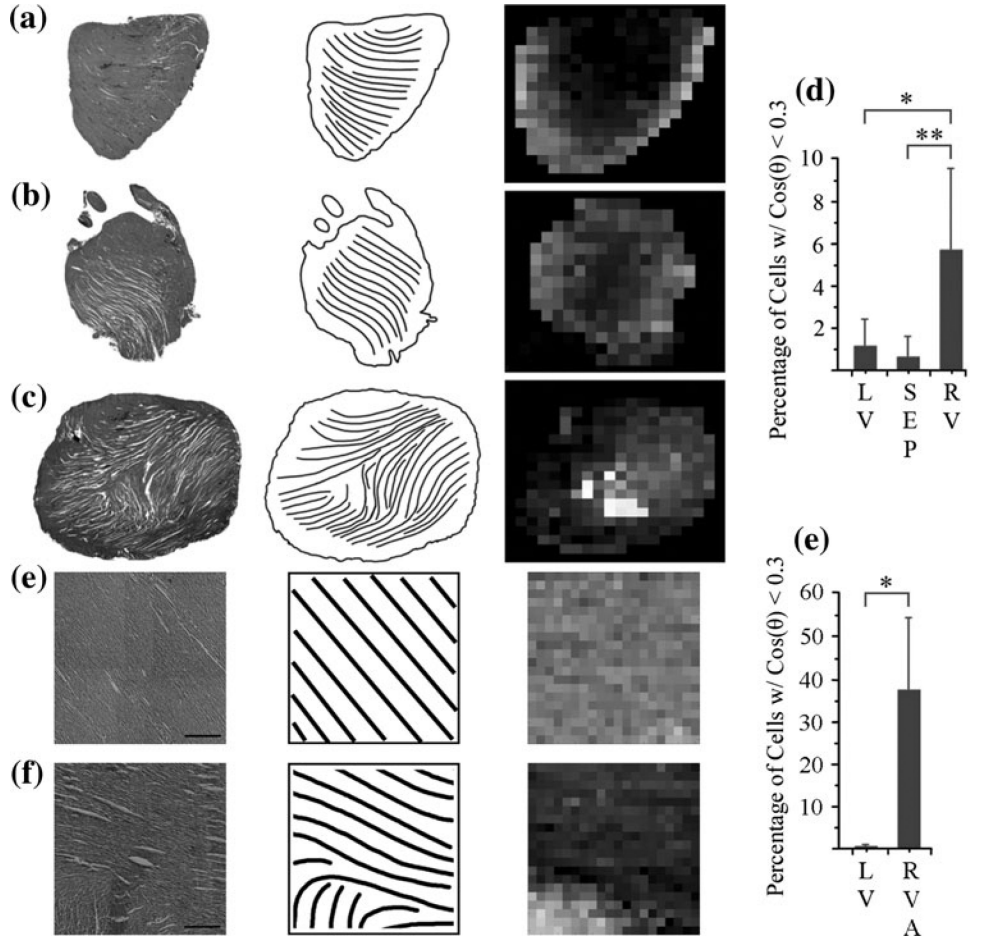


**FIGURE 5.**

Representative epicardial sections of (a) left-ventricular, (b) septal, and (c) right-ventricular regions of the rat heart, and (e) left-ventricular and (f) right-ventricular apical regions of the canine heart, with streamlines (line plots, middle column) to enhance visualization of myocyte fiber direction. Color mapping of fiber orientation in left-ventricular, septal, and right-ventricular sections (right column) shows a localization of vertical fibers (white) near the RVA region apposing fibers with a horizontal orientation (black), in contrast with the left-ventricular and septal sections. (a–c) Scale bar = 2 mm; (e–f) Scale bar = 500 $\mu$m. (d) Quantification of angle mapping in left-ventricular (LV), septal (SEP), and right-ventricular rat heart sections showing the percentage of cells where $\cos(\theta) < 0.3$. (g) Quantification of angle mapping in left-ventricular (LV) and right-ventricular canine heart sections showing the percentage of cells where $\cos(\theta) < 0.3$. *$p \leq 0.05$; **$p \leq 0.01$.

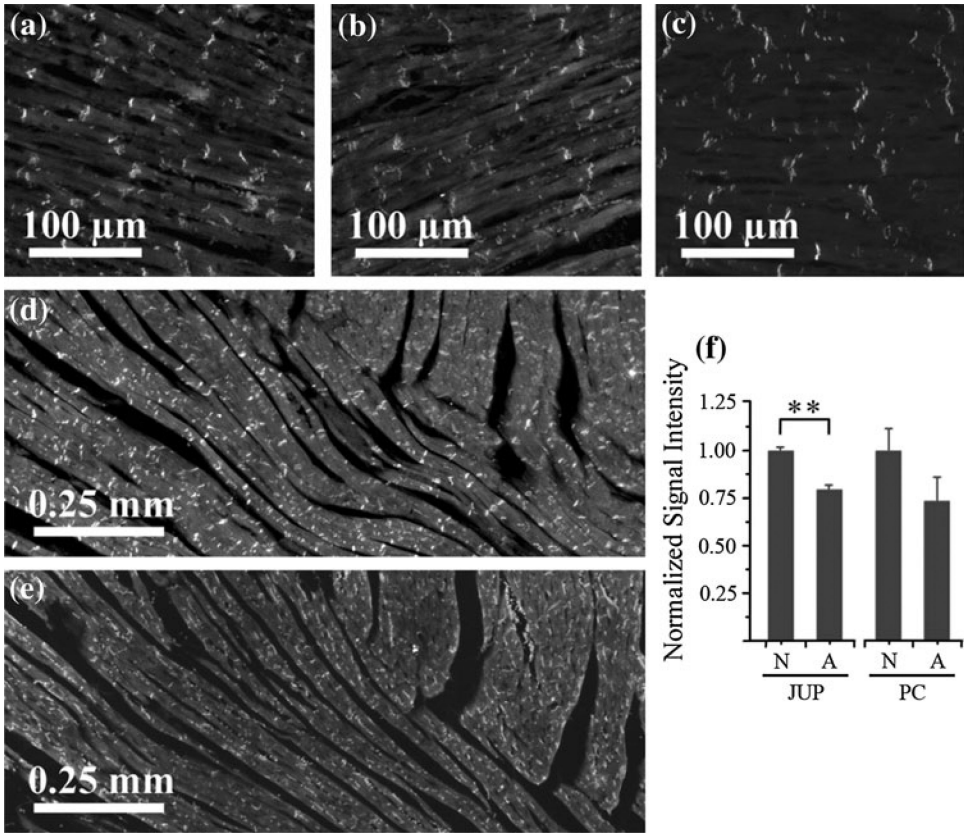


**FIGURE 6.**

(a) Left-ventricular, (b) right-ventricular, and (c) septal myocardial samples immunostained against pan-cadherin. The localization of expression is predominantly at the end-to-end junctions of the myocytes. Scale bar = 100 $\mu$m. (d) Cadherin stained region of cardiac tissue including the RVA and some tissue peripheral to the RVA. (e) Plakoglobin stained region of cardiac tissue including the RVA and some tissue peripheral to the RVA. The upper-middle region, representing the RVA, exhibits weaker staining and less organization of intercalated disks. Scale bar = 250 $\mu$m. (f) Quantification of plakoglobin (JUP) and pan-cadherin (PC) signal intensity in non-apical (N) and apical (A) regions of the right ventricle. $^{**}p \leq 0.01$.